Electric Power Systems Research 130 (2016) 89–102

Contents lists available at ScienceDirect

Electric Power Systems Research

journal homepage: www.elsevier.com/locate/epsr

Transient stability augmentation of PV/DFIG/SG-based hybrid power system by parallel-resonance bridge fault current limiter

Md. Kamal Hossain *,[1], Mohd. Hasan Ali [1]

Department of Electrical and Computer Engineering, University of Memphis, 223 Engineering Science Building, Memphis, TN 38152, USA

ARTICLE INFO

Article history:
Received 16 April 2015
Received in revised form 16 August 2015
Accepted 19 August 2015

Keywords:
Bridge type fault current limiter (BFCL)
Doubly-fed induction generator (DFIG)
Fault ride through (FRT)
Parallel-resonance bridge fault current limiter (PRBFCL)
Photovoltaic (PV)
Transient stability

ABSTRACT

This paper proposes a parallel-resonance bridge type fault current limiter (PRBFCL) to augment the transient stability of a hybrid power system consisting of a photovoltaic (PV) power generation source, a doubly-fed induction generator (DFIG)-based wind energy system, and a synchronous generator (SG). The PRBFCL is designed such a way that it can provide sufficient damping characteristics to the studied power system. The effectiveness of the proposed PRBFCL in improving the transient stability and enhancing the dynamic performance of the hybrid power system is verified by applying both balanced and unbalanced faults in the power network. Also, its performance is compared with that of the bridge type fault current limiter (BFCL) and the fault ride through (FRT) schemes, i.e. FRT schemes of PV, DFIG, and with the AVR and governor of synchronous generator (SG). Some indexes are used to quantify the system performance. Simulation results obtained from the Matlab/Simulink software show that the proposed PRBFCL is effective in maintaining stable operation of the PV, wind generator, and synchronous generator during the grid fault. Moreover, the performance of the PRBFCL is better than that of the BFCL and the FRT methods in every aspect.

1. Introduction

Rapid depletion of the traditional sources of energy as well as the perpetual increase in energy demand in today's fast growing world has made the renewable energy as a hot research topic. The cost of the photovoltaic (PV) installation is gradually becoming low, and hence its growth is proliferating day by day. Among the renewable energy sources, the solar energy will attain the top position and fulfill almost 28% of world's total energy demand by 2040 [1]. On the other hand, the wind energy generating system (WEGS) today is an established source of renewable energy with its rapid growth. Due to their numerous advantages, such as maximum power extraction [2], more efficiency, decoupled active and reactive power control, and enhanced power quality, the variable speed wind generator (VSWG) systems are gaining more popularity over conventional induction machine-based fixed-speed wind-generators. Moreover, the simple and rugged construction, low cost, ability to capture the maximum energy from a wide range of wind velocities, and partially rated ac/dc/ac converter for generating variable frequency, make the doubly fed induction generator (DFIG) the preferred choice over other wind generating systems [3].

Transient stability is the property of a power system to regain its normal operating condition following sudden and severe faults in the system [4]. The transient stability study is extremely important for maintaining the continuity of the power flow and properly controlling the modern electrical power systems with multiple renewable energy sources integrated to it.

Compared to the wind generators with full rated inverter/converters, the DFIG systems are extremely sensitive to the grid abnormalities, as their stators are directly connected to the grid. A grid side fault causes the terminal voltage of DFIG to go very low, which results in very high current through the stator and the rotor windings may hamper the stable operation and damage the machine. Several reports on minimizing the adverse effects of grid disturbances on the DFIG-based wind farms [5–11] are available in the literature, and the issues of enhancing the stability of the power networks including both wind synchronous generators (SGs) by flexible ac transmission system (FACTS) devices are addressed in [12–15]. On the other hand, the occurrence of the grid faults causes the imbalance between the PV generated power and power inserted by the voltage source inverter (VSI) to the grid. Due to this power imbalance, there is a sharp rise in intermediate DC link voltage and also an overcurrent at the AC side of the VSI, which may result in damaging of the power electronic interfaces [16]. The

* Corresponding author. Tel.: +1 901 335 8292.
E-mail address: mhssain1@memphis.edu (Md.K. Hossain).
[1] M.K. Hossain & M.H. Ali are with the Electrical & Computer Engineering Department, University of Memphis, TN 38152, USA.

http://dx.doi.org/10.1016/j.epsr.2015.08.016
0378-7796/

adverse effects of large-scale penetration of PV power to the grid on the power system stability have been reported in [17].

The integration of a large scale hybrid renewable energy plant consisting of PV, wind, and marine-current to the grid is reported in [18–20]. Large scale penetration of these renewable energy sources into the power grid leads to an enhanced short-circuit power level. Moreover, the circuit breakers with their certain turn-off capability, cannot suppress the pick current. Fault current limiters (FCLs) are extensively employed in the power system networks for suppressing the fault current. In the literature, various types of fault current limiter are proposed such as resistive-type FCLs, inductive-type FCLs, superconducting FCLs (SFCLs), flux-lock-type FCLs, DC reactor-type FCL, and resonance-type FCLs [21–26]. The application of the FCLs in the power systems is not only to suppress the peak of the short-circuit current, but also for other power system applications, such as power system transient stability augmentation, fault ride through (FRT) capability enhancement of wind generator, power quality improvement, and reliability improvement. Literature shows that coordinated operation of SFCL and SMES is employed at the PCC to enhance the FRT and the power fluctuation minimization purpose of DFIG-based wind farm [27]. Switched-type FCL and high temperature superconducting fault current limiter (HTS-FCL) are employed in [28,13], respectively, for enhancing the FRT capability of the DFIG-based wind generator. Resistor-based superconducting fault current limiter (SFCL) [25,29] and HTS-FCL [30] are placed at the PCC point in order to enhance the transient stability of synchronous generator (SG)-based single-machine-infinite-bus (SMIB) power system. Dangjin power plant, operating under utility company Korean Power Exchange (KPX), has multiple thermal power generating units connected to a common bus (PCC), and SFCL is placed at the PCC to enhance the power system stability [31].

Besides the above mentioned applications of FCLs for the stability purposes, the high-voltage direct-current (HVDC) link joined with a damping controller based on adaptive-network-based fuzzy inference system (ANFIS) utilized in [18], for enhancing the transient stability of a hybrid system consisting of PV, wind, and marine current energy generator. The static synchronous series compensator (SSSC) [32], series dynamic braking resistor (SDBR) [33], static var compensator (SVC) [34], and static synchronous compensator (STATCOM) [12] are employed for enhancing the stability of the hybrid power system consisting of DFIG, permanent magnet synchronous generator (PMSG), and SG-based power systems. Applications of SMES for enhancing the dynamic performance of grid-connected wind and PV generating systems are reported in [35].

Some of the above mentioned FCLs and other auxiliary means of enhancing the stability incur additional cost due to the use of converters, coupling transformers, and filters. SFCL employs superconducting inductor and some of the bridge-FCLs use transformer for the coupling purpose incurs high manufacturing cost. Because of the high cost of SFCLs, they are not commercially available in the markets. It is important to investigate a cost-effective and new method for transient stability improvement of hybrid power systems. Due to its simplicity and low cost, the nonsuperconducting fault current limiter [26] is a promising technique for enhancing the transient stability of the power system [36] and improving the fault ride through capability of the wind generators [37]. Resonance-type FCLs suppress the fault current by exploiting various configurations of series or parallel LC resonant circuits [38]. The resonant circuits have the advantages over solid-state circuit breakers, are the simplicity of their construction and the control strategy. The disadvantage of bridge type fault current limiter (BFCL) compared to the parallel resonant circuit fault current limiter is that, it imposes less effective impedance, because of its only current limiting inductance along with the one series resistor for the power evacuation [36]. Other BFCL topology [39] employs the coupling transformer which is an expensive approach for the fault current limiting applications. However, the impedance imposed during the fault event for PRBFCL has more impact than the BFCL, because of the presence of capacitor and multiple resistors for the power evacuation.

In this work, in order to augment the transient stability and FRT capability enhancement of a hybrid power system consisting of a DFIG-based wind generator, a PV generator, and conventional synchronous generator (SG), a parallel-resonance bridge type fault current limiter (PRBFCL) is proposed. So far, the PRBFCL has not been investigated as an auxiliary means for improving the transient stability of the power systems. During the severe voltage dips, voltage source inverter (VSI) of the PV and grid side converter (GSC) of the DFIG are utilized for the reactive current injection according to the E.ON grid code [40]. FRT scheme of PV which includes DC-link voltage suppression by controlling DC/DC boost converter of the PV system is also implemented and analyzed. Also, the performance of the proposed method is compared with that of the bridge type fault current limiter (BFCL) and fault ride through (FRT) schemes i.e. FRT schemes of PV, DFIG, and with the AVR and governor of synchronous generator (SG).

The effectiveness of the proposed scheme for enhancing the transient stability is verified by considering a test system consisting of one synchronous generator-based single machine infinite-bus system, to which one DFIG-based wind farm and a PV farm are integrated through a short transmission line. By limiting the fault current and improving the voltage sag at the point of common coupling (PCC), the proposed method makes the power sources of the hybrid system stable during the grid fault. Both balanced and unbalanced faults are applied to the most vulnerable point of the network to demonstrate the effectiveness of the proposed scheme. Extensive simulations were carried by using the Matlab/Simulink software.

The next section explains the impacts of grid fault on energy sources (PV, DFIG, and SG) of hybrid power system. The modeling of the power sources of the test system is described in Section 3. In Sections 4 and 5, the constructions and control strategies of the BFCL and the proposed method are described, respectively, and simulation results are presented in Section 6. Section 7 deals with the quantification of the results by the stability indices. The responses of the injected reactive current from the PV and the DFIG are presented in Section 8 named compliance with grid-code requirement. A brief discussion about the cost of the proposed schemes is presented in Section 9. Finally, Section 10 concludes this work.

2. Impacts of grid fault on energy sources (PV, DFIG, and SG) of hybrid power system

A three-phase two-stage grid-connected PV system, shown in Fig. 1, consists of the DC/DC converter as the first stage and the DC/AC grid-connected voltage source inverter (VSI) as the second stage. The overall power flow through the PV system can be defined by:

$$P_{PV} = P_{DC2} + P_g, \tag{1}$$

where P_{DC2} denotes the power flow through the DC-lick capacitor C_{DC2} of the PV system, P_g is the power inserted by the inverter to the grid, and P_{PV} is the PV array output. During the normal operation, the DC power generated by the PV (P_{PV}) is equal to the AC power delivered to the grid (P_g) if the power electronic converter loss is ignored:

$$P_{PV} = P_g = 3U_g I_g, \tag{2}$$

where U_g and I_g are the nominal RMS value of phase voltage and phase current, respectively. The power balance makes the PV DC-link voltage constant. However, during the event of grid-fault, the

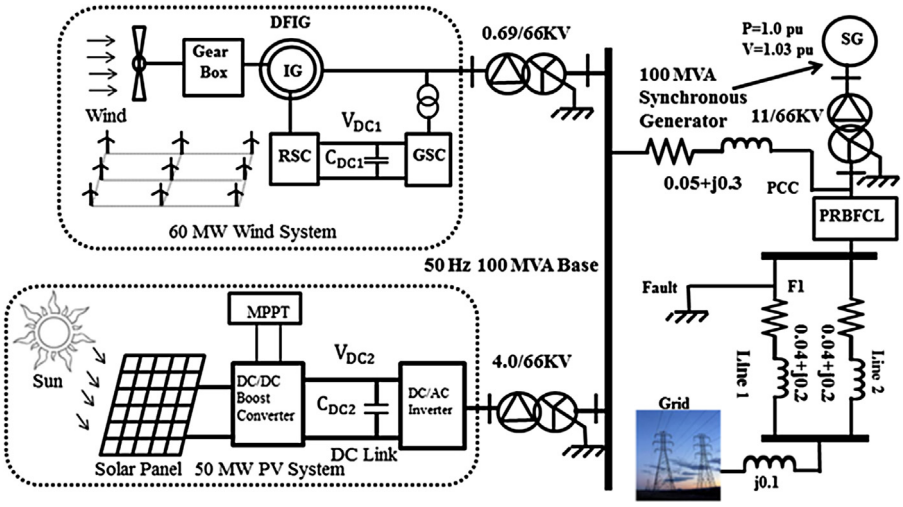

Fig. 1. Hybrid power system model.

sudden voltage sag at the PCC reduces the power inserted to the grid from P_g to P_{g_f}. Meanwhile, the DC/DC converter continues to insert the maximum possible PV power into the DC-link. The power imbalance between P_{PV} and P_{g_f} will cause the DC link voltage go high sharply. Mathematically, the condition can be expressed as follows [41]:

$$(P_{PV} - P_{g\_f})\Delta t = P_{DC2}\Delta t = \frac{1}{2}C_{DC2}(V_{DC2\_f}^2 - V_{DC2}^2) \quad (3)$$

where V_{DC2} and V_{DC2_f} are the amplitudes of the DC-link voltage before and during the fault, respectively, and Δt represents the duration of the fault. Exploiting (2) and (3) and considering $P_{g\_f} = 3\,V_f\,I_g$, the DC-link voltage during the fault can be derived as

$$V_{DC2\_f} = \sqrt{\frac{2(P_{PV} - 3V_f I_g)\Delta t}{C_{DC2}} + V_{DC2}^2}, \quad (4)$$

It can be seen from (4), the deeper the voltage sag (V_f goes low during the grid-fault) and the longer the fault duration are, the larger the rising rate of the PV DC-link voltage will be. Therefore, without any protection scheme the drop in the PCC voltage during the fault may cause the over-voltage violation at the DC-link.

During the network fault, fault current is fed from power sources to the faulty node due to huge voltage sag at that node which causes very small active power and voltage generation at the rotating machines (DFIG & SG). That leads the rotating machines of the system to lack of the equilibrium state and may incur the instability. This situation can be explained by the swing equation as follows [13]:

$$\frac{2H}{\omega}\frac{d^2\delta}{dt^2} = P_m - P_e \quad (5)$$

where P_m is the input mechanical power, P_e is the output electrical power, δ is the rotor angle and H is the inertia constant of the machine. From (5), it can be seen that the stability of the machine can be maintained by making the output electrical power equivalent to the mechanical power. The impedance introduced by the PRBFCL during the fault causes the stator voltage of the DFIG and SG to be developed due to voltage drop across the impedance of the PRBFCL. Delivery of the electrical power is maintained by DFIG and SG, and the desired power balance is achieved.

3. System model

This work employed the power system model depicted in Fig. 1 for transient stability and dynamic performance analysis. It consists of one synchronous generator (100 MVA, SG)-based single machine infinite-bus system [41–44], to which one PV farm of 50 MW and one DFIG-based wind farm of 60 MW are integrated through a short transmission line. These energy sources are delivering power to the utility grid through double circuit transmission lines. Although a practical wind power station consists of many generators, it is considered to contain a large equivalent aggregated single generator with the power capacity mentioned in the paper. The wind generator is driven by an equivalent aggregated variable-speed wind turbine (VSWT) through an equivalent gearbox [12]. Also, the PV plant consists of a large number of PV modules connected in series-parallel combination to attain the desired power level, and it is connected to the PCC by a boost converter and an equivalent aggregated dc to ac inverter. The perturb and observe (P&O) maximum power point tracker (MPPT) [45] for the PV is implemented on the boost converter for extracting maximum PV power at varying meteorological conditions. The PRBFCL or BFCL is placed at the grid point as shown in Fig. 1.

3.1. Modeling of PV system

The equivalent circuitry of a PV array is shown in Fig. 2, in which the simple model can be represented by the current sources, diodes, and the resistors (R_S and R_P). Here, resistors signify the non-ideal behavior of the PV module. Large PV plants are composed of several PV panels or modules. In this work, 100 PV modules are connected in series, and total 2500 branches are connected in parallel to form a PV plant of rated 50 MW. KC200GT PV module with 200 W of peak power is employed for this work [46].

3.2. Controlling of boost converter

At normal operating condition, the MPPT generates the duty cycle to drive the DC/DC boost converter. When there is a grid fault, the DC-link voltage goes to very high, as the incoming DC power from the PV panel cannot be injected to the grid, due to severe

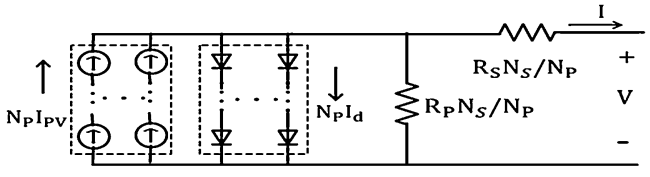

Fig. 2. Equivalent circuit of PV array.

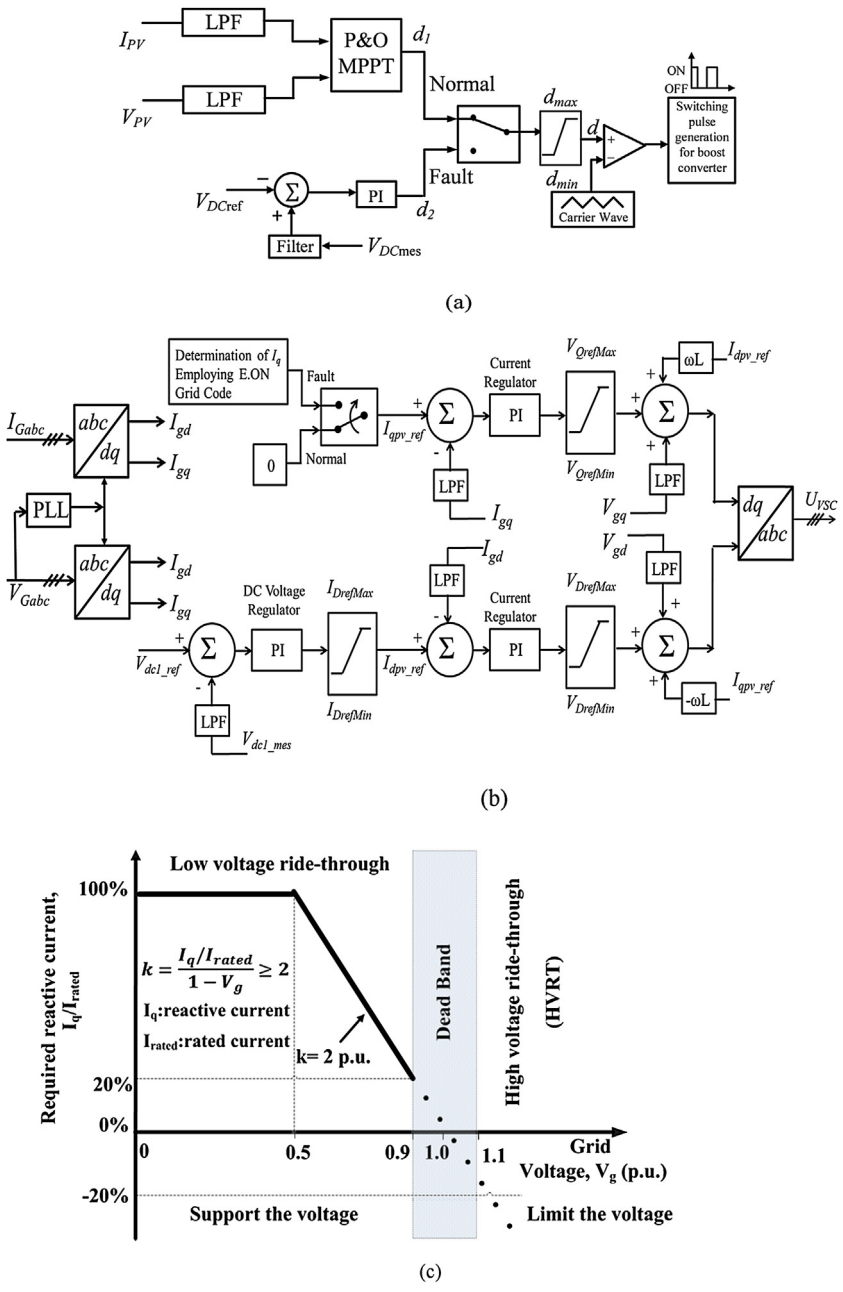

Fig. 3. (a) Control scheme of DC-DC boost converter of PV, (b) control scheme of voltage source inverter of PV, (c) injected reactive current profile by PV inverter.

voltage dip. In order to mitigate the sharp rise in PV DC-link voltage, a non-MPPT mode is adopted as shown in Fig. 3(a) [16,41,47]. The MPPT controller is bypassed, and the PI controller-based non-MPPT strategy comes into the action, when the grid fault is detected. The non-MPPT strategy reduces the active power insertion to the grid during emergency grid fault, which will eventually allow the inverter to insert reactive current to provide dynamic voltage support without exceeding the inverter maximum current limit.

3.3. Controlling of voltage source inverter (VSI)

In this work, a three-level, three-phase voltage source inverter (VSI) is used for the conversion of DC power to AC power for grid interfacing. Fig. 3(b) represents the control strategy of the VSI along with the reactive power injection scheme according to the grid code [16,41,47]. The VSI control system employs external voltage regulator for generating I_{dpv_ref} reference current for maintaining constant DC link voltage. I_{qpv_ref} is set to zero for maintaining the unity power factor at normal operating condition. When a voltage sag is appeared due to grid side fault, the reactive current injected according to the E.ON grid code [40], as shown in Fig. 3(c), and mathematically it can be expressed as [48]:

$$\frac{I_q}{I_n} = \begin{cases} 0, & 0.9\,\text{pu} \leq V_g \leq 1.1\,\text{pu} \\ k - kV_g, & 0.5\,\text{pu} \leq V_g \leq 0.9\,\text{pu} \\ 1, & V_g \leq 0.5\,\text{pu} \end{cases} \quad (6)$$

where the value of k is 2 and V_g is the PCC voltage, I_q is the reference reactive current and I_n is the rated inverter current. According to the E.ON grid code, the VSI should insert full reactive current when

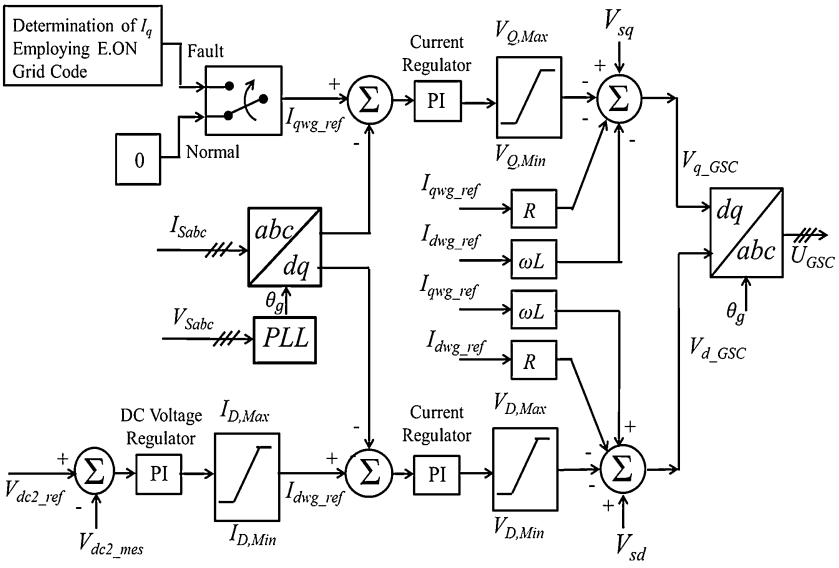

Fig. 4. Control system for the DFIG grid side converter.

grid voltage drops down to 0.5 pu. The reference reactive current during the voltage dip can be determined by:

$$I_{\text{qpv\_ref}} = \frac{I_q}{I_n} \times I_n \tag{7}$$

The reference active current during the fault condition can be determined by [41]:

$$I_{\text{dpv\_ref}} = \begin{cases} I_n, & 0.9\,\text{pu} \le V_g \le 1.1\,\text{pu} \\ \sqrt{I_n{}^2 - I_{\text{qpv\_ref}}^2}, & 0.5\,\text{pu} \le V_g \le 0.9\,\text{pu} \\ 0, & V_g \le 0.5\,\text{pu} \end{cases} \tag{8}$$

The internal current regulator generates the desired direct ($V_{\text{d\_VSC}}$) and quadrature ($V_{\text{q\_VSC}}$) axis voltage which are then converted to three modulating voltage to VSC control. The control scheme describe above is sufficient to perform FRT of the PV system during the grid disturbance.

3.4. Modeling of synchronous generator

The equations employed to model the SG in this work are described in [4]. The SG is equipped with automatic voltage regulator (AVR) and Governor (GOV) control systems [49]. The SG parameters employed for the design consideration are available in [49]. Subtransient effects are taken into consideration while designing the SG model. The model is designed considering the rotor dq-axis as reference which rotates at rotor speed.

3.5. Modeling of wind turbine

The mechanical power extraction from the wind can be expressed as follows [50].

$$P_w = 0.5 * \rho * \pi * R^2 * V_w^3 * C_P(\lambda, \beta) \tag{9}$$

where P_w and V_w are the extracted power (watt) from the wind and the wind velocity (m s^{-1}) respectively, ρ represents the air density [kg m^{-3}], and C_p denotes the power coefficient which is the function of tip speed ratio, λ, and blade pitch angle, β [°], and R represents

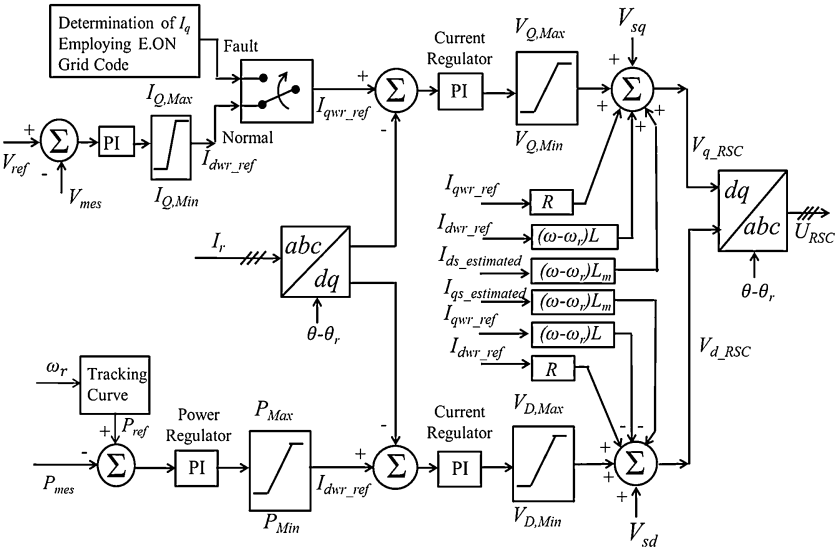

Fig. 5. Control system for the DFIG rotor side converter.

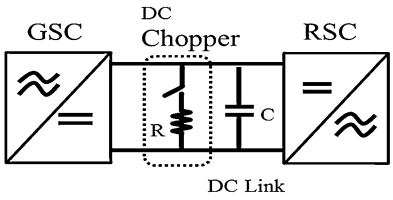

Fig. 6. DFIG DC-link protection scheme with DC chopper.

the blade radius in meter (m). Also, the wind turbine MOD-2 model is considered for this work [13].

3.6. Control scheme of DFIG

The DFIG stator winding is connected to the grid by 0.69/66 kV step-up transformer, whereas the rotor winding is connected to the low voltage side of the step-up transformer through the power electronic converters (rotor side converter (RSC) and grid side converter (GSC) and a transformer. A DC link is connected between the RSC and GSC. The DFIG has the provision of independent control of active and reactive powers by employing rotor and grid side converters [12]. The GSC is used to maintain a constant DC link voltage and regulate the stator voltage as shown in Fig. 4. The measured current in the dq frame (I_{ds_mes} and I_{qs_mes}) needs to track the reference current I_{d_ref} and I_{q_ref}, respectively, to maintain constant DC link voltage and unity power factor at the output of the GSC converter. During the normal operation, I_{q_ref} is set to zero; however, during the grid fault, the reference reactive current is determined by E.ON grid code, as described in PV reactive current insertion strategy. The desired direct (V_{d_GSC}) and quadrature (V_{q_GSC}) axis voltage is generated by the current regulator. Fig. 5 demonstrates the control mechanism of RSC. The control of RSC needs the measured rotor current in dq frame (I_{drw_mes} and I_{qrw_mes}) to track the reference currents that are generated by the real power and the magnitude of the stator voltage setting, respectively. For this case also, a current regulator is employed to generate the desired direct (V_{d_RSC}) and quadrature (V_{q_RSC}) axis voltage [12].

3.7. Protection of the DC-link of DFIG during fault

A DC-chopper with a resistor is connected in parallel with the DC-link of the DFIG as shown in Fig. 6., with a similar function to that of the rotor side crowbar for the purpose of reducing the DFIG dc-link voltage during the fault [33]. During the grid voltage sag, the additional active power coming from the rotor side converter is dissipated at the DC chopper, and the abrupt rise of DC link voltage is prevented. The IGBT is ON when V_{DC1} exceeds V_{DC1max}, and thus, the DC chopper is switched ON and the energy is consumed by the resistance.

4. Bridge type fault current limiter (BFCL)

In this work, in order to see the effectiveness of the proposed PRBFCL, its performance is compared with that of the bridge type fault current limiter (BFCL) [36,51]. The BFCL was employed for enhancing the fault ride through capability [39] of wind firm and the transient stability [36] of multimachine power system.

4.1. BFCL configuration, design and control

Fig. 7 shows the bridge fault current limiter (BFLC) [36]. It consists of two branches: bridge part and shunt branch. The construction of the bridge part is same as that of the PRBFCL. During the normal operation, closed IGBT switch permits the positive half line current to pass through the diodes D_1, D_4 and, bridge part; whereas,

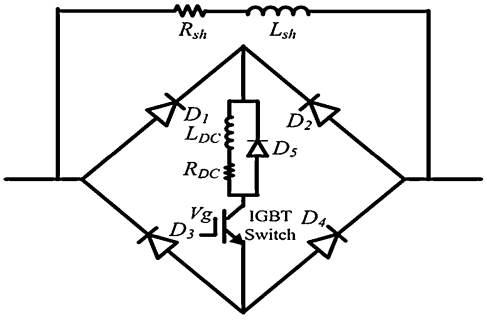

Fig. 7. Bridge fault current limiter.

the negative half cycle of the line current flows through D_3, L_{DC}, switch and D_2. During the fault event at the transmission line, the IGBT switch is opened by the controller that forces the line current to take the path of shunt branch. For designing the shunt branch, the strategy adopted in [51] is implemented in the work. To minimize the negative impact of the grid fault to the power sources, BFCL needs to consume the power at least equal to the power carried by the line at prefault condition. By consuming the power generated by the power sources during the grid fault BFCL minimizes the destabilizing torque of the rotating machines and also makes the power balance between DC and AC sides of the VSI of the static PV generator. The value of X_{Sh} and R_{sh} are found to be 0.014 pu and 0.488 pu, respectively for obtaining best system performance. In [51], the procedure for determining the values of X_{sh} and R_{sh} are discussed in detail. The control structure of the BFCL is same as that of the PRBFCL as shown in Fig. 9. Although the control structures for both PRBFCL and BFCL are the same, but the impedance imposed during the fault event for PRBFCL has more impact than the BFCL, because of the presence of capacitor and resistor.

5. Parallel-resonance bridge fault current limiter (PRBFCL)

5.1. Configuration of PRBFCL

Fig. 8 shows the configuration of PRBFCL which consists of two branches, namely, bridge part and resonance branch. The bridge part consists of a diode rectifier bridge, a small dc link inductor (L_{dc}), an IGBT-based semiconductor and a freewheeling diode (D_5). It is worthwhile to mention here that high rating diodes (Semikron SKNa 402 and VS-SD1700C.K [52]) and semiconductor (IGBT) switches (CM200HG-130H) are commercially available [51]. In general, the bridge could be made up of more than one diode per branch (in series or in parallel) and that in the proposed example one diode is sufficient for sustaining the entire power in normal operation. For example, the VS-SD1700C.K [52] series diode has maximum rated current above 3 kA and the maximum current that

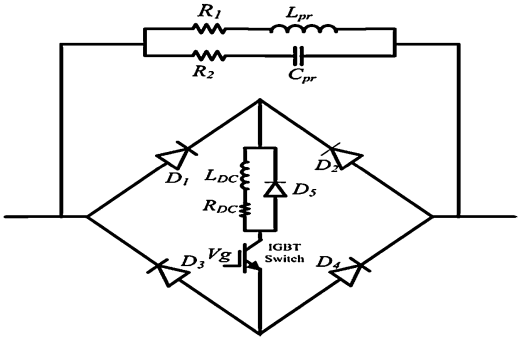

Fig. 8. Configuration of PRBFCL.

can flow through the PRBFCL is 1.83 kA. Also, for the protection of the semiconductor switch, a snubber circuit is required which is not shown here. The other branch of PRBFCL contains parallel resonance part of LC and two series connected resistors with L and C, respectively.

5.2. PRBFCL design

The model system power capacity is taken into the consideration for approximating the parameters of the PRBFCL. The current characteristic of IGBT is employed to choose the value of L_{DC}. In this work, as a protection scheme, the PRBFCL is placed in each phase of three-phase line near to the PCC. Since the maximum capacity of the hybrid power system is 210 MW, each phase of the three-phase line carries 70 MW of maximum power. To ensure the normal operation, the parallel-resonance (PR) branch should hold the PCC voltage near to the prefault voltage. The effective resistance of the PRBFCL (R_{PR}) allows the evacuation of the active power of hybrid power system; it also creates a voltage drop that leads to boosting the terminal voltage of the power sources. The power consumed by the PRBFCL at postfault is given by:

$$P_{PRBFCL} \le \frac{P_G}{3} \tag{10}$$

$$P_{PRBFCL} \le I^2_{fault} R_{PR} \tag{11}$$

where P_G ($P_G = P_{Solar} + P_{Wind} + P_{SG}$) represents the rated power generated by the hybrid source and P_{Solar}, P_{Wind}, and P_{SG} represent the rated power generated by solar, wind, and synchronous generator, respectively; R_{PR} is the PRBFCL equivalent resistance required to consume the generated source power. The value of R_{PR} is about 0.48 pu considering (10) and (11).

For the sake of numerical explanation for getting the value of R_{PR} equal to 0.48 pu, it is considered that each phase of the three-phase line carries 70 MW (210 MW/3) of maximum power. In this condition, the predesired value of the fault current (1.83 kA) can be achieved by considering the equal sign of Eqs (10) and (11) as follows:

$$P_{PRBFCL} = \frac{210\,\text{MW}}{3} = 70\,\text{MW}, I_{fault} = (70\,\text{MW}/66\text{kV}) * \text{sqrt}(3) = 1.83\,\text{kA},$$

$R_{PR} = (70\,\text{MW}/(1.83\,\text{kA})^2)/R_{base} = 0.48$ pu, where $R_{base} = V^2{}_{nom}/P_{base}$; R_{base} = base resistance, P_{base} = system base power.

The inequity sign in (10) and (11) come into the consideration when the renewable energy sources generate less power than that of their rated capacities. In that case, power consumed by the PRBFCL (P_{PRBFCL}) satisfies the conditions $P_{PRBFCL} < P_g/3$ and $P_{PRBFCL} < I^2{}_{fault} R_{PR}$, or $R_{PR} > P_{PRBFCL}/I^2{}_{fault}$. Renewable energy sources such as PV and wind could generate less power than that of their rated capacities because of the varying environmental conditions (low irradiance for PV and low wind speed). Considering the SG always delivers 100 MW of base power, the value of P_{PRBFCL} varies from 33.33 MW (100 MW/3, 100 MW from SG and 0 MW from PV and wind generator) to 70 MW (210 MW/3, 100 MW from SG and 110 MW from PV and wind generator). It is important to note here that the value of R_{PR} is determined considering all energy sources in the hybrid power system generate rated power. From the simulation results, it is found that the same design consideration of PRBFCL is also capable of stabilizing the hybrid system, when the renewable energy sources do not produce the rated capacity power. The variations of the R_{PR} can be demonstrated in the following Table 1:

The derivation of the equivalent impedance of the resonant part is as follows:

$$Z_{PR} = \frac{R_1 R_2 + (L_{pr}/C_{pr})}{R_1 + R_2} + j\frac{\omega L_{pr}(R_2 - R_1)}{R_1 + R_2} \tag{12}$$

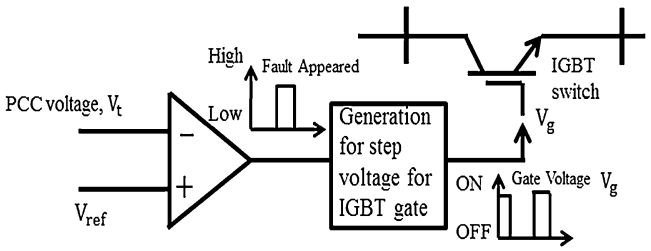

Fig. 9. Control scheme of PRBFCL/BFCL.

The resistive part of Z_{PR} is made equal to the R_{PR} (0.48 pu), considering the rated power generated by the energy sources of hybrid power system.

$$R_{PR} = \frac{R_1 R_2 + (L_{pr}/C_{pr})}{R_1 + R_2} \tag{13}$$

A standard capacitor (C_{pr}) value of 300 μF is selected from [53] for the system voltage level. An inductor (L_{pr}) value of 0.0338 H is computed considering the resonance condition with 50 Hz operating frequency. For the design consideration, the value of R_2 is chosen as 1.15 pu [14,51,54] and then the value of R_1 calculated from (13) is 0.73 pu. Also, the value of L_{dc} used for this work is 1 mH with the inherent resistance R_{DC} of 0.3 mΩ which results in time constant of 3.33 s and this is suitable enough to make the DC reactor current smooth. It is important to note here that the design parameters mentioned here are the same for both balanced and unbalanced faults in order to evaluate the transient stability of the hybrid power system.

5.3. Control of PRBFCL

At the time of normal operation, the IGBT switch remains on state, since the gate voltage V_g is high and the positive half line current passes through D_1, L_{DC}, R_{DC} and D_4. For the negative half cycle, current conduction takes place in D_2, L_{DC}, R_{DC}, and D_3. L_{DC} imposes negligible voltage drop at the time of normal operation, since it has a very small value. The current through the bridge is unidirectional or DC, which causes L_{DC} to charge at peak current and behaves like a short circuit. Therefore, the bridge has no impact at normal system operation. The resonance branch imposes high impedance at power frequency to allow any leakage current.

Fig. 9 represents the control scheme of the PRBFCL. Normally, the overcurrent at PCC or voltage dip at PCC is employed to detect the fault or grid abnormality in case of grid-connected PV system [50]. In this work, voltage at PCC is exploited for fault detection and PRBFCL control mechanism. When the fault is appeared on the line, the PCC voltage goes near to zero and the PRBFCL control system makes the IGBT gate voltage to go low that eventually turns off the IGBT. The bridge is open-circuited and parallel-resonance branch come into the action with the faulted line. The resonance branch limits the fault current and holds the PCC voltage up to make the PV, wind and synchronous generator dynamically stable. At the same time the freewheeling diode (D_5) gives the discharge path of L_{DC}, when the IGBT switch turns off. As the circuit breaker opens and system recovers, the PCC voltage rises. When the PCC voltage regains to the level of nominal voltage, the gate voltage goes high to turn on the IGBT and system returns its normal operation. Also, at fault initiation, the L_{DC} acts as a current snubber, which hinders the sharp rise of di/dt to protect the IGBT. Depending on the output of the comparator, a step generator generates the proper get voltage to turn on or turn-off the IGBT switch.

Table 1
Determination of R_{PR}.

P_{SG} (constant power contribution)	$P_{Solar} + P_{Wind}$ (variable power contribution)	Total power generated by hybrid system $P_{SG} + P_{Solar} + P_{Wind}$	Per phase power $(P_{SG} + P_{Solar} + P_{Wind})/3$ or P_{PRBFCL} during fault	I_{fault}	R_{PR} (1 pu = 43.57 ohm)
100 MW	0 MW	100 MW	33.33 MW	0.87 kA	1 pu or 43.57 ohm
100 MW	40 MW	140 MW	46.67 MW	1.22 kA	0.71 pu or 31.12 ohm
100 MW	80 MW	180 MW	60 MW	1.57 kA	0.55 pu or 24.2 ohm
100 MW	110 MW	210 MW	70 MW	1.83 kA	0.48 pu or 20.9 ohm

6. Simulation result and discussion

6.1. Simulation scenario

In this work, simulations were carried out by using the Matlab/Simulink Software. For the transient analysis, both balanced [three-line-to-ground (3LG)] and unbalanced [double-line-to ground (2LG) and line-to-ground (1LG)] faults were considered at F1 location near the PCC as shown in Fig. 1. Fault location F1 is the most vulnerable point of the network since it is the closest point to the PRBFCL device. The fault is considered to occur at 0.1 s, the breakers of the lines are opened at 0.2 s (after 5 cycles) and reclosed at 1.2 s (after 50 cycles). A total simulation time of 10 s with 0.00001 s time step is considered. Simulations are conducted for following three cases:

1) Case 1: without any auxiliary controller
2) Case 2: with PRBFCL
3) Case 3: with BFCL
4) Case 4: with FRT schemes (FRT of PV + FRT of DFIG + AVR and GOV schemes of SG)

6.2. Transient stability improvement by PRBFCL during balanced fault

The transient stability performance of the energy sources in the hybrid power system is evaluated when the system is subjected to a bolted 3LG (three-line-to-ground) fault at F1 location in Fig. 1. The comparative simulation results of DFIG and SG are shown in Figs. 10 and 11, respectively. The real power inserted to the grid during the fault by DFIG and SG, without series protection schemes, drops down to very low, as illustrated in Figs. 10(c) and 11(b), respectively. Hence, the mechanical power of the DFIG and SG cannot be transformed into electrical power that causes a very high stresses on the mechanical parts of the rotating machines (DFIG and SG) and increasing the DFIG and SG rotor speed, as shown in Figs. 10(a) and 11(b), respectively. Without any protection scheme in the system, the current rises abruptly and the voltage drop occurs at the wind generator and SG terminals during the fault. The electromagnetic torque of the DFIG abruptly goes near to the zero, since the electromagnetic torque is proportional to the square of the terminal voltage [55]. During the grid fault, the PRBFCL or BFCL suppresses the fault current and prevents the DFIG and SG terminal voltages to go low, as shown in Figs. 10(b) and 11(d), respectively. With employing the PRBFCL or BFCL, the DFIG and the SG are able to deliver the real power to the grid and keep the generators near to equilibrium condition according to (5). Without any series protection scheme (i.e. FRT or no controller schemes), the equilibrium condition of the rotating machines is not maintained; consequently the rotor speed is increased. It is evident from the comparative transient responses of DFIG and SG represented in Figs. 10 and 11 that, the PRBFCL offers better transient stability than the system with BFCL. From the Figs. 10 and 11, it can be observed that SG and DFIG demonstrate less oscillatory behavior during the disturbance by

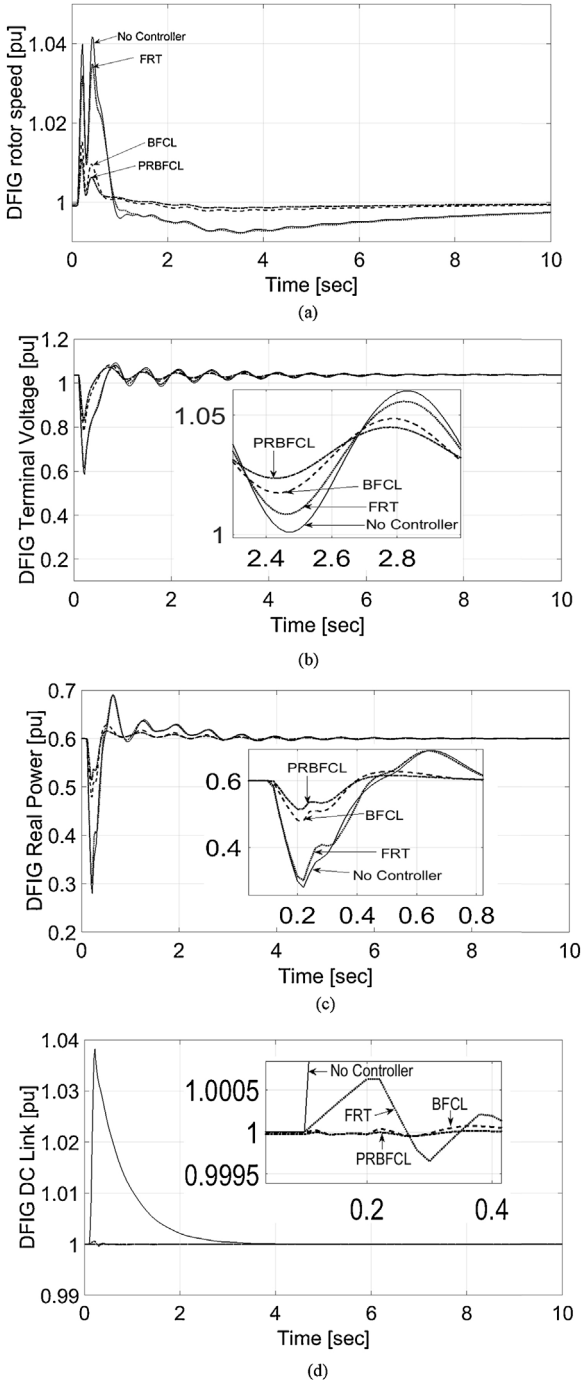

Fig. 10. (a)–(d) Responses of DFIG without compensation, with FRT schemes, with BFCL, and with PRBFCL in response to 3LG fault at F1 location.

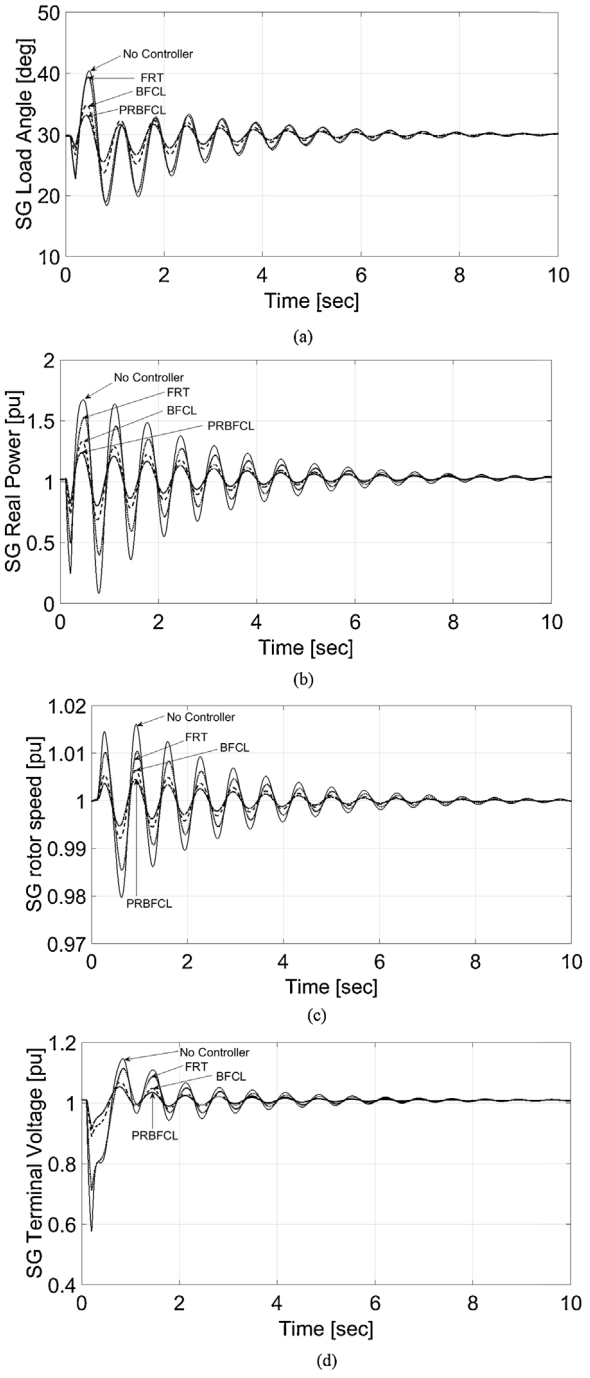

Fig. 11. (a)–(d) Responses of SG without compensation, with FRT schemes, with BFCL, and with PRBFCL in response to 3LG fault at F1 location.

the FRT schemes compared to that of the no controller scheme. Since the FRT schemes of PV and DFIG are accompanied with the reactive current injection according to the PCC voltage dip, it also helps damping the electromechanical oscillations as evident from Figs. 10 and 11.

The grid side fault causes the oscillations in the voltage and current of DC side of the PV voltage source inverter (VSI) [56] (Fig. 12). The VSI requires a constant DC link voltage and the oscillation is not desirable for its proper functioning. When a fault occurs, the inverter is unable to deliver the power generated by the PV plant to the grid because of the drop in the grid voltage. The excess energy gives a sharp rise to the DC link voltage. Also, the low voltage due to grid fault prevents the full transmission of generated real power

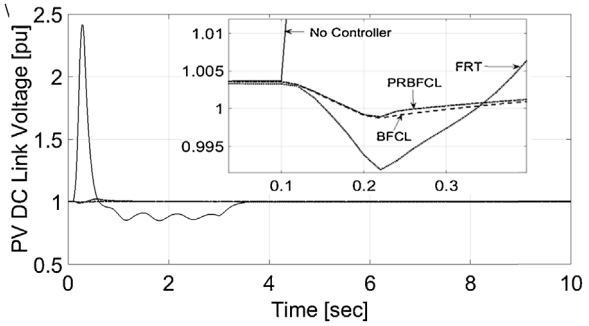

Fig. 12. Comparative transient responses PV DC-link voltage considering the studied system subject to 3LG fault at F1 location.

from the wind turbine to the grid, leading to power imbalance between RSC and GSC of DFIG that causes the rising of the DC-link voltage, and increasing fluctuations of the currents and voltages in the DFIG system [57]. Although the DC-link overvoltage of PV and DFIG are mitigated by the internal controllers installed in the stations themselves (i.e. Non-MPPT voltage regulator for PV and DC-chopper circuit for DFIG), the proposed PRBFCL helps improving the DC-link profiles of both the DFIG and the PV as shown in Figs. 11(d) and 12, respectively. Oscillation of the DC-link voltages are damped down after clearing the fault by breaker opening and controller tracks the nominal DC-link voltage. Comparative simulation results of the hybrid power system considering a 3LG fault at the middle of the transmission line 2 is shown in Fig. 13. It is evident from the simulation results of Fig. 13 that, the series protection scheme of PRBFCL is more effective than BFCL in stabilizing the hybrid power system considering severe fault at the middle of the transmission line.

6.3. Transient stability improvement by PRBFCL during unbalanced fault

Stability analysis regarding the unbalanced fault conditions are also investigated under the proposed protection scheme. The responses of the DFIG-based wind generator, PV system and SG in case of the 2LG and 1LG faults at F1 location of the studied power system are shown in Figs. 14 and 15, respectively. It is clear from the Figs. 14 and 15 that the transient stability of the power sources are enhanced by both the PRBFCL and BFCL in the case of unbalanced fault. However, the PRBFCL performs better than the BFCL.

7. Index based transient stability performance

For more clear perspective, transient stability of the hybrid system is evaluated by exploiting several performance indices, such as, dfig_{pow}(pu.sec), dfig_{vlt} (pu.sec), dfig_{spd} (pu.sec), sg_{ang}, (deg.sec), sg_{pow}(pu.sec), sg_{vlt} (pu.sec), sg_{spd} (pu.sec), and PV_{vlt} (v.sec). Lower values of the indices indicate improved system performance. Mathematical representations of the performance indices of the power generating sources can be defined as follows:

$$\text{dfig}_{\text{pow}}(\text{pu. sec}) = \int_0^T \left|\Delta P_{\text{wg}}\right| dt \tag{14}$$

$$\text{dfig}_{\text{vlt}}(\text{pu. sec}) = \int_0^T \left|\Delta V_{\text{wg}}\right| dt \tag{15}$$

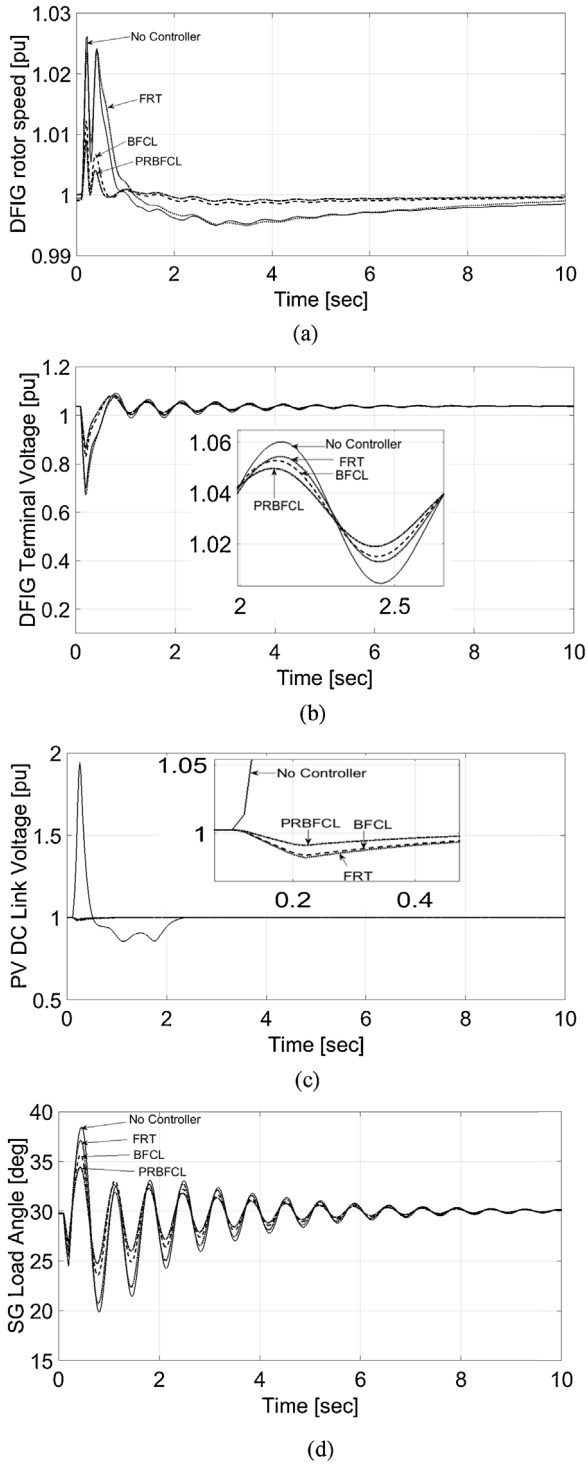

Fig. 13. Comparative transient responses of the power system under 3LG fault at the middle of the second transmission line. (a) Equivalent DFIG-based wind farm rotor speed, (b) equivalent DFIG-based wind farm terminal voltage, (c) PV DC-link voltage, (d) SG load angle.

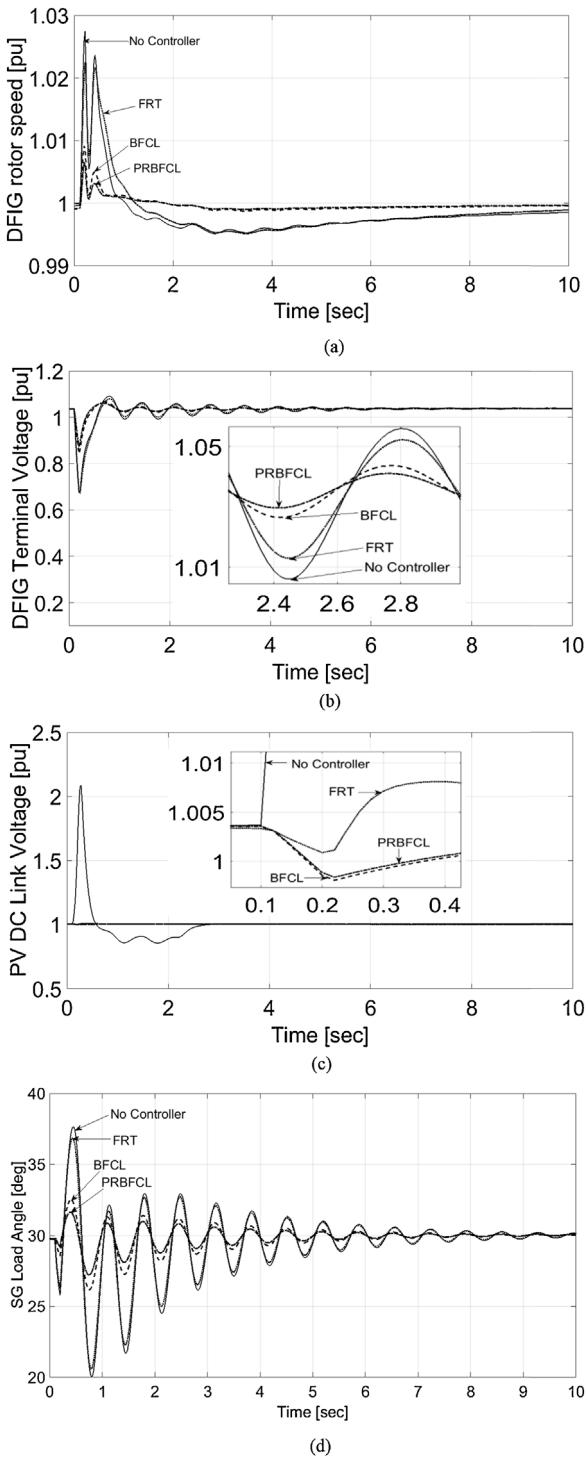

Fig. 14. Comparative transient responses of the power system under 2LG fault at F1 location. (a) Equivalent DFIG-based wind farm rotor speed, (b) equivalent DFIG-based wind farm terminal voltage, (c) PV DC-link voltage, (d) SG load angle.

$$\mathrm{dfig}_{\mathrm{spd}}(\mathrm{pu.sec}) = \int_0^T \left|\Delta\omega_{\mathrm{wg}}\right| dt \tag{16}$$

$$\mathrm{PV}_{\mathrm{vlt}}(\mathrm{pu.sec}) = \int_0^T \left|\Delta V_{\mathrm{pvdc}}\right| dt \tag{17}$$

$$\mathrm{sg}_{\mathrm{ang}}(deg.\,\mathrm{sec}) = \int_0^T \left|\Delta\delta\right| dt \tag{18}$$

$$sg_{\mathrm{pow}}(\mathrm{pu.sec}) = \int_0^T \left|\Delta P_{\mathrm{sg}}\right| dt \tag{19}$$

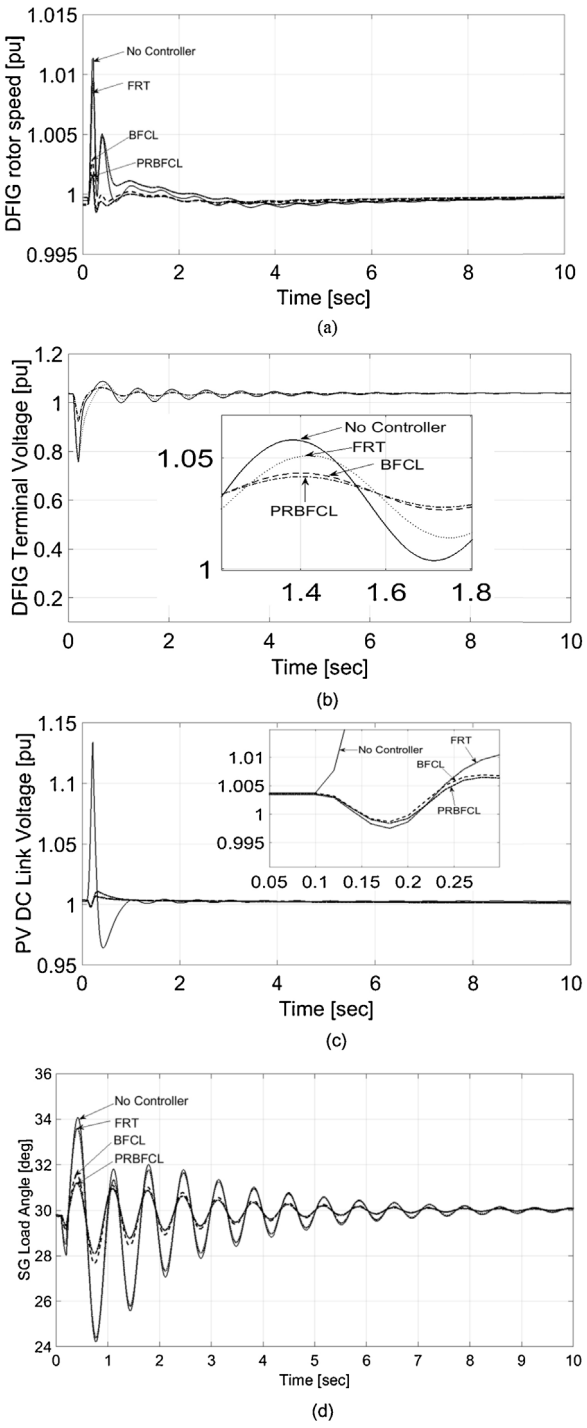

Fig. 15. Comparative transient responses of the power system under 1LG fault at F1 location. (a) Equivalent DFIG-based wind farm rotor speed, (b) equivalent DFIG-based wind farm terminal voltage, (c) PV DC-link voltage, (d) SG load angle.

$$\mathrm{sg_{vlt}(pu.\,sec)} = \int_0^T \left|\Delta V_{\mathrm{sg}}\right| dt \tag{20}$$

$$\mathrm{sg_{spd}(pu.\,sec)} = \int_0^T \left|\Delta \omega_{\mathrm{sg}}\right| dt \tag{21}$$

where ΔP_{wg}, ΔV_{wg}, $\Delta \omega_{\mathrm{wg}}$, ΔV_{pvdc}, $\Delta \delta$, ΔP_{sg}, ΔP_{sg}, and $\Delta \omega_{\mathrm{sg}}$ represent power deviation of DFIG, terminal voltage deviation of DFIG, speed deviation of DFIG, DC-link voltage deviation of PV, the load angle deviation of SG, power deviation of SG, terminal voltage deviation of SG, and rotor speed deviation of SG, respectively. Also, T is the total simulation time of 10.0 s. Tables 2–4 represent the values of the indices for the 3LG, 2LG, and 1LG faults, respectively. It is evident from Tables 2–4 that the system performance is the worst without any protection scheme. However, a notable improvement in stability performance can be observed with the PRBFCL and BFCL in the system. Also, compared to BFCL and FRT methods, the PRBFCL shows smaller stability indices, which means it performs better for stabilization of the system.

Table 2
Values of indices for performance comparison during 3LG fault.

Index parameters	Values of indices			
	Without controller	With FRT	With BFCL	With PRBFCL
$\mathrm{dfig_{spd}}$ (pu.sec)	0.167	0.166	0.117	0.109
$\mathrm{dfig_{pow}}$ (pu.sec)	0.279	0.278	0.221	0.210
$\mathrm{dfig_{vlt}}$ (v.sec)	0.330	0.319	0.231	0.212
$\mathrm{pv_{vlt}}$ (pu.sec)	0.855	0.201	0.186	0.181
$\mathrm{sg_{ang}}$ (deg.sec)	18.17	16.68	9.502	6.707
$\mathrm{sg_{vlt}}$ (pu.sec)	0.322	0.296	0.158	0.115
$\mathrm{sg_{spd}}$ (pu.sec)	0.105	0.104	0.101	0.098
$\mathrm{sg_{pow}}$ (pu.sec)	1.829	1.691	1.039	0.773

Table 3
Values of indices for performance comparison during 2LG fault.

Index parameters	Values of indices			
	Without controller	With FRT	With BFCL	With PRBFCL
$\mathrm{dfig_{spd}}$ (pu.sec)	0.147	0.146	0.107	0.105
$\mathrm{dfig_{pow}}$ (pu.sec)	0.254	0.251	0.206	0.203
$\mathrm{dfig_{vlt}}$ (pu.sec)	0.283	0.278	0.208	0.200
$\mathrm{pv_{vlt}}$ (pu.sec)	0.656	0.187	0.176	0.172
$\mathrm{sg_{ang}}$ (deg.sec)	14.86	13.56	5.186	3.454
$\mathrm{sg_{vlt}}$ (pu.sec)	0.257	0.238	0.094	0.069
$\mathrm{sg_{spd}}$ (pu.sec)	0.113	0.103	0.101	0.100
$\mathrm{sg_{pow}}$ (pu.sec)	1.543	1.415	0.632	0.479

8. Compliance with grid-code requirement

The PV and wind generator have to insert mandatory reactive current during PCC voltage drop. The E.ON grid-code requirement for the reactive current insertion by the PV and wind generator during the voltage sag is shown in Fig. 3(c). Accordingly, PV and wind generators have to supply full (100%) reactive current when the voltage falls below 50%. The performance of the proposed protection scheme is evaluated in conjunction with the E.ON grid code for the voltage profile and reactive current support during the 3LG fault. Fig. 16(a) and (b) shows the reactive current profiles of the PV and DFIG, respectively, during 3LG fault (100% voltage dip) with the protection schemes. The PV plant injects full reactive current of 1 pu as directed in Fig. 16(a), while the reactive current insertion from GSC of DFIG reaches its rated limit of 0.3 pu with respect to rated capacity of the wind farm with all the protection schemes as shown in Fig. 16(b). Normally, the rated capacity of the converter is 30% or 0.3 pu with respect to the rated capacity of the wind firm which allows only 0.3 pu reactive power to be injected during 3LG with 100% voltage dip.

9. Cost and practical implementation feasibility

Although the actual cost of the PRBFCL and BFCL are not known, however, it can be inferred from the number of components used for the device fabrication. A single phase implementation of the PRBFCL requires resistor, capacitor, inductor, diodes and the power

Table 4
Values of indices for performance comparison during 1LG fault.

Index parameters	Values of indices			
	Without controller	With FRT	With BFCL	With PRBFCL
$dfig_{spd}$ (pu.sec)	0.115	0.108	0.104	0.103
$dfig_{pow}$ (pu.sec)	0.219	0.214	0.201	0.200
$dfig_{vlt}$ (pu.sec)	0.227	0.212	0.195	0.191
pv_{vlt} (pu.sec)	0.241	0.185	0.174	0.162
sg_{ang} (deg.sec)	8.301	7.592	3.280	2.556
sg_{vlt} (pu.sec)	0.143	0.136	0.063	0.053
sg_{spd} (pu.sec)	0.120	0.112	0.098	0.095
sg_{pow} (pu.sec)	0.919	0.845	0.466	0.408

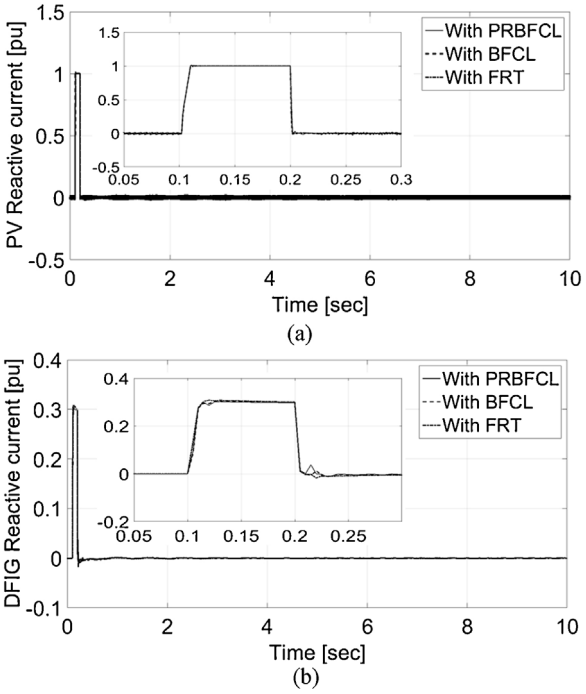

Fig. 16. Reactive current injection due to 3LG fault with 100% voltage dips: (a) injected reactive current from the VSI of the PV into the grid; (b) injected reactive current from the GSC into the grid.

electronic switches. With the advancement of the power electronics application, the high rating IGBT switches and power diodes are available in the market for the practical implementation of PRBFCL. Also, the capacitor, inductor and resistor are simple and inexpensive passive electrical components. Therefore, the total establishment cost for the PRBFCL might be little higher than that of BFCL, since it requires one more resistor and capacitor. So, the PRBFCL can be installed with the large-scale power generators connected to the grid to sustain and obtain the stability of the energy sources during the grid abnormality.

10. Conclusion

This paper proposes the application of a PRBFCL to enhance the transient stability of a large scale hybrid system consisting of a wind generator, a PV system, and a synchronous generator. The effectiveness of the proposed method is tested by considering both balanced and unbalanced faults at one of the transmission lines. Based on simulations, the following points are noteworthy.

a) The proposed PRBFCL method ensures the transient stability augmentation of the hybrid power system.
b) The impact of the proposed protection scheme is significant in stabilizing the rotating machines in the hybrid power system, such as SG and DFIG.
c) Internal FRT scheme is sufficient for stabilizing the low-inertia PV generators in the hybrid power system.
d) The performance of PRBFCL is better than that of BFCL which is evident from the graphical plots as well as index values.

In our future work, we will look into other protection and stabilizing devices and design the damping controller for enhancing the power system stability.

Appendix A.

A.1. PV modeling equations

For any given array formed by Nser × Npar identical modules, the equivalent *I–V* characteristics can be expressed as follows [46]:

$$I = I_{PV}N_{par} - I_0 N_{par}\left[e\left(\frac{V + R_S(N_{ser}/N_{par})I}{V_t a N_{ser}}\right) - 1\right] - \frac{V + R_S(N_{ser}/N_{par})I}{R_P(N_{ser}/N_{par})} \quad (22)$$

where V and I represent the PV module output voltage and current, respectively. $V_t = N_S kT/q$ is the thermal voltage of the module and N_s is the number of series connected solar cell in a module.

A.2. Doubly fed induction generator modeling equations

The mathematical representation of the DFIG is important for its coordinated control. The governing voltage equations for DFIG in rotating dq reference frame can be given by [13,50]:

$$\begin{bmatrix} V_{ds} \\ V_{qs} \\ V_{dr} \\ V_{qr} \end{bmatrix} = \begin{bmatrix} R_s & 0 & 0 & 0 \\ 0 & R_s & 0 & 0 \\ 0 & 0 & R_r & 0 \\ 0 & 0 & 0 & R_r \end{bmatrix} \begin{bmatrix} I_{ds} \\ I_{qs} \\ I_{dr} \\ I_{qr} \end{bmatrix} + \frac{d}{dt} \begin{bmatrix} \lambda_{ds} \\ \lambda_{qs} \\ \lambda_{dr} \\ \lambda_{qr} \end{bmatrix}$$

$$+ \begin{bmatrix} -\omega_1\lambda_{qs} \\ \omega_1\lambda_{qs} \\ -(\omega_1 - \omega_2)\lambda_{qr} \\ (\omega_1 - \omega_2)\lambda_{dr} \end{bmatrix} \begin{bmatrix} \lambda_{ds} \\ \lambda_{qs} \\ \lambda_{dr} \\ \lambda_{qr} \end{bmatrix} = \begin{bmatrix} L_s & 0 & L_m & 0 \\ 0 & L_s & 0 & L_m \\ L_m & 0 & L_r & 0 \\ 0 & L_m & 0 & L_r \end{bmatrix} \begin{bmatrix} I_{ds} \\ I_{qs} \\ I_{dr} \\ I_{qr} \end{bmatrix} \quad (23)$$

where the symbols s, r, d, q, V, I, λ represent the stator, rotor d axis and q axis, voltage, current and flux linkage respectively. R_s and R_r denote the stator and rotor resistance, respectively. ω_1 and ω_2 represent supply and rotor angular frequency, respectively, whereas

L_s and L_r are the stator and rotor leakage inductance, respectively, and L_m is the magnetizing inductance.

The DFIG stator output active (P_S) and reactive (Q_S) powers are given by [13]

$$P_S = \frac{3}{2}(V_{ds}I_{ds} + V_{qs}I_{qs}) \quad (24)$$

$$Q_S = \frac{3}{2}(V_{qs}I_{ds} - V_{ds}I_{qs}) \quad (25)$$

References

[1] T.J. Hammons, Integrating renewable energy sources into European grids, Int. J. Electr. Power Energy Syst. 30 (2008) 462–475, http://dx.doi.org/10.1016/j.ijepes.2008.04.010.

[2] E. Muljadi, C.P. Butterfield, J. Chacon, H. Romanowitz, Power quality aspects in a wind power plant, in: 2006 IEEE Power Eng. Soc. Gen. Meet., 2006, p. 8, http://dx.doi.org/10.1109/PES.2006.1709244.

[3] H. Li, Z. Chen, Overview of different wind generator systems and their comparisons, IET Renew. Power Gener. 2 (2008) 123, http://dx.doi.org/10.1049/iet-rpg:20070044.

[4] P. Kundur, Power System Stability and Control, McGraw-Hill, New York, NY, USA, 2006, http://dx.doi.org/10.1049/ep.1977.0418.

[5] L. Wang, K.H. Wang, Dynamic stability analysis of a DFIG-based offshore wind farm connected to a power grid through an HVDC link, IEEE Trans. Power Syst. 26 (2011) 1501–1510, http://dx.doi.org/10.1109/TPWRS.2010.2085053.

[6] L. Wang, L.-Y. Chen, Reduction of power fluctuations of a large-scale grid-connected offshore wind farm using a variable frequency transformer, IEEE Trans. Sustain. Energy 2 (2011) 226–234, http://dx.doi.org/10.1109/TSTE.2011.2142406.

[7] F.M. Hughes, O. Anaya-Lara, N. Jenkins, G. Strbac, A power system stabilizer for DFIG-based wind generation, IEEE Trans. Power Syst. 21 (2006) 763–772, http://dx.doi.org/10.1109/TPWRS.2006.873037.

[8] I. Erlich, J. Kretschmann, J. Fortmann, S. Mueller-Engelhardt, H. Wrede, Modeling of wind turbines based on doubly-fed induction generators for power system stability studies, IEEE Trans. Power Syst. 22 (2007) 909–919, http://dx.doi.org/10.1109/TPWRS.2007.901607.

[9] A.D. Hansen, G. Michalke, Fault ride-through capability of DFIG wind turbines, Renew. Energy 32 (2007) 1594–1610, http://dx.doi.org/10.1016/j.renene.2006.10.008.

[10] M. Rahimi, M. Parniani, Transient performance improvement of wind turbines with doubly fed induction generators using nonlinear control strategy, IEEE Trans. Energy Convers. 25 (2010) 514–525, http://dx.doi.org/10.1109/TEC.2009.2032169.

[11] B. Pokharel, W. Gao, Mitigation of disturbances in DFIG-based wind farm connected to weak distribution system using STATCOM, in: North Am. Power Symp. 2010, NAPS, 2010, http://dx.doi.org/10.1109/NAPS.2010.5619587.

[12] L. Wang, D.N. Truong, Stability enhancement of DFIG-based offshore wind farm fed to a multi-machine system using a STATCOM, IEEE Trans. Power Syst. 28 (2013) 2882–2889, http://dx.doi.org/10.1109/TPWRS.2013.2248173.

[13] S. Alarai, S. Member, A. Moawwad, S. Member, M. Shawky, E. Moursi, et al., Voltage Booster Schemes for Fault Ride-Through Enhancement of Variable Speed Wind Turbines, vol. 4, 2013, pp. 1071–1081.

[14] M.S. El Moursi, K. Goweily, J.L. Kirtley, M. Abdel-Rahman, Application of series voltage boosting schemes for enhanced fault ridethrough performance of fixed speed wind Turbines, IEEE Trans. Power Deliv. 29 (2014) 61–71, http://dx.doi.org/10.1109/TPWRD.2013.2287398.

[15] R.G. Wandhare, V. Agarwal, Novel stability enhancing control strategy for centralized PV-grid systems for smart grid applications, IEEE Trans. Smart Grid (2014), http://dx.doi.org/10.1109/TSG.2013.2279605.

[16] F. Yang, L. Yang, X. Ma, An advanced control strategy of PV system for low-voltage ride-through capability enhancement, Sol. Energy 109 (2014) 24–35, http://dx.doi.org/10.1016/j.solener.2014.08.018.

[17] S. Eftekharnejad, V. Vittal, G.T. Heydt, B. Keel, J. Loehr, Impact of increased penetration of photovoltaic generation on power systems, Power Syst. IEEE Trans. 28 (2013) 893–901, http://dx.doi.org/10.1109/TPWRS.2012.2216294.

[18] L. Wang, M.S.N. Thi, Stability enhancement of large-scale integration of wind, solar, and marine-current power generation fed to an sg-based power system through an lcc-hvdc link, IEEE Trans. Sustain. Energy 5 (2014) 160–170, http://dx.doi.org/10.1109/TSTE.2013.2275939.

[19] H. Lund, Large-scale integration of optimal combinations of PV, wind and wave power into the electricity supply, Renew. Energy 31 (2006) 503–515, http://dx.doi.org/10.1016/j.renene.2005.04.008.

[20] D.A. Halamay, T.K.A. Brekken, A. Simmons, S. McArthur, Reserve requirement impacts of large-scale integration of wind, solar, and ocean wave power generation, IEEE Trans. Sustain. Energy 2 (2011) 321–328, http://dx.doi.org/10.1109/TSTE.2011.2114902.

[21] D. Ito, E.S. Yoneda, K. Tsurunaga, T. Tada, T. Hara, T. Ohkuma, et al., 6.6 kV/1.5 kA-class superconducting fault current limiter development, IEEE Trans. Magn. 28 (1992) 438–441, http://dx.doi.org/10.1109/20.119905.

[22] D.W.A. Willen, J.R. Cave, Short circuit test performance of inductive high T_c superconducting fault current limiters, IEEE Trans. Appl. Supercond. 5 (1995), http://dx.doi.org/10.1109/77.402731.

[23] H. Ohsaki, M. Sekino, S. Nonaka, Characteristics of resistive fault current limiting elements using YBCO superconducting thin film with meander-shaped metal layer, in: IEEE Trans. Appl. Supercond., 2009, pp. 1818–1822, http://dx.doi.org/10.1109/TASC.2009.2019040.

[24] S.H. Lim, H.S. Choi, D.C. Chung, Y.H. Jeong, Y.H. Han, T.H. Sung, et al., Fault current limiting characteristics of resistive type SFCL using a transformer, IEEE Trans. Appl. Supercond. (2005) 2055–2058, http://dx.doi.org/10.1109/TASC.2005.849450.

[25] B.C. Sung, D.K. Park, J.-W. Park, T.K. Ko, Study on a series resistive SFCL to improve power system transient stability: modeling, simulation, and experimental verification, IEEE Trans. Ind. Electron. 56 (2009) 2412–2419, http://dx.doi.org/10.1109/TIE.2009.2018432.

[26] M.T. Hagh, M. Abapour, Nonsuperconducting fault current limiter with controlling the magnitudes of fault currents, IEEE Trans. Power Electron. 24 (2009) 613–619, http://dx.doi.org/10.1109/TPEL.2008.2004496.

[27] I. Ngamroo, T. Karaipoom, Cooperative Control of SFCL and SMES for Enhancing Fault Ride Through Capability and Smoothing Power Fluctuation of DFIG Wind Farm, vol. 24, 2014.

[28] W. Guo, L. Xiao, S. Dai, Y. Li, X. Xu, et al., LVRT capability Eenhancement of DFIG with switch-type fault current limiter, IEEE Trans. Ind. Electron. 62 (2015) 332–342.

[29] M. Tsuda, Y. Mitani, K. Tsuji, K. Kakihana, Application of resistor based superconducting fault current limiter to enhancement of power system transient stability, IEEE Trans. Appl. Supercond. (2001) 2122–2125, http://dx.doi.org/10.1109/77.920276.

[30] S.M. Alaraifi, M.S. El Moursi, Hybrid HTS-FCL configuration with adaptive voltage compensation capability, IEEE Trans. Appl. Supercond. 24 (2014) 1–8, http://dx.doi.org/10.1109/TASC.2014.2329392.

[31] S. Seo, S.J. Kim, Y.H. Moon, B. Lee, A hybrid superconducting fault current limiter for enhancing transient stability in Korean power systems, Physica C: Supercond. Appl. 494 (2013) 331–334, http://dx.doi.org/10.1016/j.physc.2013.04.025.

[32] T. Dinh-Nhon, Designed damping controller for SSSC to improve stability of a hybrid offshore wind farms considering time delay, Electr. Power Energy Syst. 65 (2015) 425–431.

[33] K.E. Okedu, S.M. Muyeen, R. Takahashi, J. Tamura, Wind farms fault ride through using DFIG with new protection scheme, IEEE Trans. Sustain. Energy 3 (2012) 242–254, http://dx.doi.org/10.1109/TSTE.2011.2175756.

[34] L. Wang, S. Member, D. Truong, Stability Enhancement of a Power System with a PMSG-based and a DFIG-based Offshore Wind Farms Using a SVC with an Adaptive-Network-based Fuzzy Inference System, vol. 60, 2011, pp. 2799–2807.

[35] S.T. Kim, B.K. Kang, S.H. Bae, J.W. Park, Application of SMES and grid code compliance to wind/photovoltaic generation system, IEEE Trans. Appl. Supercond. 23 (2013) 4, http://dx.doi.org/10.1109/tasc.2012.2232962.

[36] M. Jafari, S.B. Naderi, M.T. Hagh, M. Abapour, S.H. Hosseini, Voltage sag compensation of point of common coupling (PCC) using fault current limiter, IEEE Trans. Power Deliv. 26 (2011) 2638–2646, http://dx.doi.org/10.1109/TPWRD.2011.2161496.

[37] M.E. Elshiekh, D.A. Mansour, A.M. Azmy, Improving fault ride-through capability of DFIG-based wind turbine using superconducting fault current limiter, IEEE Trans. Appl. Supercond. 23 (2013), http://dx.doi.org/10.1109/TASC.2012.2235132, 5601204-5601204.

[38] C. Meyer, R.W. De Doncker, LCC analysis of different resonant circuits and solid-state circuit breakers for medium-voltage grids, IEEE Trans. Power Deliv. 21 (2006) 1414–1420, http://dx.doi.org/10.1109/TPWRD.2005.861334.

[39] M. Firouzi, G.B. Gharehpetian, Improving fault ride-through capability of fixed-speed wind turbine by using bridge-type fault current limiter, IEEE Trans. Energy Convers. 28 (2013) 361–369, http://dx.doi.org/10.1109/TEC.2013.2248366.

[40] I. Erlich, H. Brakelmann, Integration of Wind Power into the German High Voltage Transmission Grid, in: 2007 IEEE Power Eng. Soc. Gen. Meet., 2007, http://dx.doi.org/10.1109/PES.2007.385790.

[41] W. Kou, D. Wei, P. Zhang, W. Xiao, A direct phase-coordinates approach to fault ride through of unbalanced faults in large-scale photovoltaic power systems, Electr. Power Compon. Syst. 43 (2015) 902–913, http://dx.doi.org/10.1080/15325008.2015.1014580.

[42] L. Wu, R. Takahashi, M. Nakagawa, T. Murata, J. Tamura, A basic study of wind generator stabilization with doubly-fed asynchronous machine, IEEJ Trans. Power Energy 124 (2004) 1101–1110, http://dx.doi.org/10.1541/ieejpes.124.1101.

[43] M.H. Ali, B. Wu, Comparison of stabilization methods for fixed-speed wind generator systems, IEEE Trans. Power Deliv. 25 (2010) 323–331, http://dx.doi.org/10.1109/TPWRD.2009.2035423.

[44] M.H. Ali, M. Park, I.K. Yu, T. Murata, J. Tamura, Improvement of wind-generator stability by fuzzy-logic-controlled SMES, IEEE Trans. Ind. Appl. 45 (2009) 1045–1051, http://dx.doi.org/10.1109/TIA.2009.2018901.

[45] M.K. Hossain, M.H. Ali, Overview on maximum power point tracking (MPPT) techniques for photovoltaic power systems, Int. Rev. Electr. Eng. 8 (2013) 1363–1378.

[46] M.G. Villalva, J.R. Gazoli, E.R. Filho, Comprehensive approach to modeling and simulation of photovoltaic arrays, IEEE Trans. Power Electron. 24 (2009) 1198–1208, http://dx.doi.org/10.1109/tpel.2009.2013862.

[47] S.I. Nanou, S.A. Papathanassiou, Modeling of a PV system with grid code compatibility, Electr. Power Syst. Res. 116 (2014) 301–310, http://dx.doi.org/10.1016/j.epsr.2014.06.021.

[48] Y. Yang, S. Member, P. Enjeti, F. Blaabjerg, Suggested Grid Code Modifications to Ensure Wide-Scale Adoption of Photovoltaic Energy in Distributed Power Generation Systems, 2015.
[49] M.H. Ali, Wind Energy Systems: Solutions for Power Quality and Stabilization, CRC Press, Boca Raton, FL, USA, 2012.
[50] X. Liu, P. Wang, P.C. Loh, A hybrid AC/DC microgrid and its coordination control, IEEE Trans. Smart Grid 2 (2011) 278–286, http://dx.doi.org/10.1109/TSG.2011.2116162.
[51] G. Rashid, M.H. Ali, Transient Stability Enhancement of Doubly Fed Induction Machine-Based Wind Generator by Bridge-Type Fault Current Limiter, 2015, pp. 1–9.
[52] Vishay Semiconductors. [Online]. Available: http://www.vishay.com/docs/93539/vs-sd1700ckseries.pdf.
[53] A. Ioinovici, Switched-capacitor power electronics circuits, IEEE Circuits Syst. Mag. 1 (2001) 37–42, http://dx.doi.org/10.1109/7384.963467.
[54] M.K. Hossain, M.H. Ali, Low voltage ride through capability enhancement of grid connected PV system by SDBR, in: IEEE PES T&D Conf Expo., 2014, pp. 1–5.
[55] S.M. Muyeen, R. Takahashi, M.H. Ali, T. Murata, J. Tamura, Transient stability augmentation of power system including wind farms by using ECS, IEEE Trans. Power Syst. 23 (2008) 1179–1187, http://dx.doi.org/10.1109/TPWRS.2008.920082.
[56] P.P. Dash, M. Kazerani, Dynamic modeling and performance analysis of a grid-connected current-source inverter-based photovoltaic system, IEEE Trans. Sustain. Energy. 2 (2011) 443–450, http://dx.doi.org/10.1109/TSTE.2011.2149551.
[57] L. Yang, Z. Xu, J. Østergaard, Z.Y. Dong, K.P. Wong, Advanced control strategy of DFIG wind turbines for power system fault ride through, IEEE Trans. Power Syst. 27 (2012) 713–722, http://dx.doi.org/10.1109/TPWRS.2011.2174387.